ELSEVIER

Contents lists available at ScienceDirect

Science of the Total Environment

journal homepage: www.elsevier.com/locate/scitotenv





Gestational exposure to carbon black nanoparticles triggered fetal growth restriction in mice: The mediation of inactivating autophagy-lysosomal degradation system in placental ferroptosis

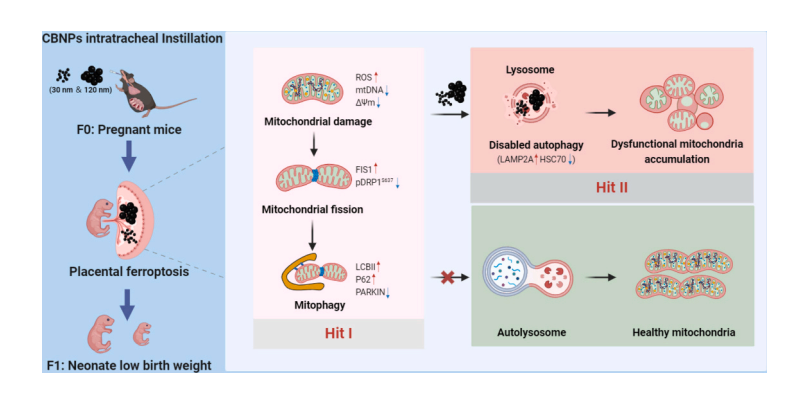
Jing Li ^{a,1}, Hongying Gao ^{a,1}, Zehua Xu ^{a,1}, Biling Gao ^a, Liang Zhang ^d, Bowen Su ^a, Shijing Yang ^a, Jiangling Liu ^a, Ya Liu ^a, Xiuxiu Wang ^e, Heng Wang ^c, Yi Lin ^{a,*}, Heqing Shen ^{a,b,**}

- ^a State Key Laboratory of Vaccines for Infectious Diseases, Xiang An Biomedicine Laboratory & State Key Laboratory of Molecular Vaccinology and Molecular Diagnostics, School of Public Health, Xiamen University, Xiamen 361102, China
- ^b Department of Obstetrics, Women and Children's Hospital, School of Medicine, Xiamen University, Xiamen 361003, China
- ^c Zhoushan Municipal Center for Disease Control and Prevention, Zhoushan, Zhejiang 316021, China
- d Department of Neurosurgery and Department of Neuroscience, Fujian Key Laboratory of Brain Tumors Diagnosis and Precision Treatment, Xiamen Key Laboratory of Brain Center, The First Affiliated Hospital of Xiamen University, School of Medicine, Xiamen University, Xiamen 361102, China
- e College of the Environment and Ecology, Xiamen University, Xiamen 361102, China

HIGHLIGHTS

- CBNPs could enter mice's placenta via intratracheal instillation.
- CBNPs inflicted placental mitochondria and autophagy dysfunction.
- CBNPs inflicted placental ferroptosis by mitochondrial and autophagy disruption.
- CBNPs evoked placental ferroptosis, ultimately leading to fetal growth restriction.

GRAPHICAL ABSTRACT



ARTICLE INFO

Editor: Daqiang Yin

Keywords: Carbon black nanoparticles Mitochondria Autophagy Ferroptosis

ABSTRACT

Carbon black nanoparticles (CBNPs) are ubiquitous in our daily ambient environment, either resulting from tobacco combustion or constituting the core of $PM_{2.5}$. Despite the potential risk of trafficking CBNPs to the fetus, the underlying toxicity of nano-sized carbon black particles in the placenta remains unambiguous. Pregnant C57BL/6 mice received intratracheal instillation of 30 nm or 120 nm CBNPs. CBNPs deposited in the lungs could infiltrate the red blood cells, further cross into the placenta, and cause fetal growth restriction. Mechanistically, we proposed a two-hit hypothesis in placenta response to CBNPs. The first hit was that CBNPs caused

^{*} Correspondence to: Yi Lin, School of Public Health, Xiamen University, Xiang'an South Road, Xiamen 361102, China.

^{**} Correspondence to: H. Shen, School of Public Health, Women and Children's Hospital School of Medicine, Xiamen University, Xiang'an South Road, Xiamen 361102, China.

E-mail addresses: leejing@stu.xmu.edu.cn (J. Li), 32620211150853@stu.xmu.edu.cn (Z. Xu), tjlinyi@xmu.edu.cn (Y. Lin), hqshen@xmu.edu.cn (H. Shen).

 $^{^{1}\,}$ The authors contribute equally to this work.

Placenta Fetal growth restriction mitochondrial damage, reflected in the reduced mitochondrial matrix, the excessive mitochondrial fission, and the decreased mitochondrial membrane potential and mtDNA copy number. The second hit was that CBNPs disrupted the autophagy-lysosomal degradation system, impeding the removal of dysfunctional mitochondria and resulting in ferroptosis. Ferrestatin-1, a ferroptosis inhibitor, and rapamycin, an autophagy promotor, reversed ferroptosis and further confirm our suspicion. The findings suggested that CBNPs-triggered double-hit evoked placental ferroptosis, leading to fetal growth restriction. The study raised concerns about the potential placental toxicity of CBNPs and its impact on the fetal adverse outcome, which may propose potential targets for interventions in placental damage.

1. Introduction

Carbon black nanoparticles (CBNPs) have been extensively utilized in the fields of novel materials, environment, energy, and biomedicine owing to their beneficial properties of superior mechanical robustness, pliability, ductility, and adaptable thermal and electrical conductivities (Bacakova et al., 2020; Brunella et al., 2021; Andrade-Guel et al., 2022; Torrinha et al., 2020). CBNPs have been identified as the core of some fine and ultrafine particulate matters (i.e., PMs of PM_{2.5} and PM_{0.1}) (Hou et al., 2020). Also, tobacco combustion could generate carbon black nanoparticles (Chang et al., 2022). As part of combustion-derived particulate matter, carbon-related particles have been measured in the human placenta (Bové et al., 2019). Therefore, CBNPs-induced potential placental toxicity has raised concerns.

The human placenta sits at the interface between maternal and fetal vascular beds, which mediates the nutrient and waste exchange to maintain fetal health (Maltepe and Fisher, 2015). Trophoblasts are important cells to support the regulation of placental homeostasis and normal function, which can be damaged by nanoparticles (Manojlović-Stojanoski et al., 2022; Yang et al., 2022). Studies showed that black carbon could accumulate in the human placenta and affect the placenta homeostasis (Zhao et al., 2021; Deyssenroth et al., 2021; Van Pee et al., 2023). Besides, the rising PM concentration increased the risk of preterm birth, low birth weight, and high newborn blood pressure (Lakshmanan et al., 2015; van Rossem et al., 2015). Compared with PM2.5, the smaller size PM_{0.1} can generate greater threats to public health due to the greater surface area and reactivity (Mukherjee and Agrawal, 2018; Terzano et al., 2010). However, the molecular mechanism of nano-sized carbon black particles-induced placental toxicity has not been elucidated.

Mitochondria have been suggested as the target organelle of PM exposure in the placental cells (Li et al., 2019). Maintaining healthy and functional mitochondria in the placenta is vital during gestation to respond to stress conditions (Sferruzzi-Perri et al., 2019). Mitochondrial dysfunction is reflected as increased mitochondrial fission, decreased mitochondrial membrane potential, and decreased mitochondrial DNA content. All these may result in placenta injury and adverse birth outcomes (Xu et al., 2021; Gillmore et al., 2022). In the present work, we hypothesized that mitochondrial damage was involved in the CBNPs-induced placental damage.

Multiple studies have demonstrated that exposure to PM increases autophagy, which is an evolutionarily conserved process of self-cellular component recycling (Deng et al., 2013; Chen et al., 2016; Liu et al., 2022). Autophagy plays a dual role in the impairment caused by PM exposure (Wu et al., 2021; Liu et al., 2023a). Mitophagy may play a protective role against inflammation (Zhang et al., 2020). While, PM-induced autophagy could enhance pulmonary fibrosis (Kaushik and Cuervo, 2018). PARKIN plays a central role in mitochondrial quality control, which mediates mitophagy upon environmental pollutants exposure (Zhong et al., 2021; Zhang et al., 2020). Besides, chaperonemediated autophagy (CMA), as a special form of autophagy, is quite different from macroautophagy in terms of its cargo selectivity and delivery (Kaushik and Cuervo, 2018). CMA performs intracellular regulation by degrading damaged or harmful proteins. CMA substrates are recognized and targeted by a cytosolic chaperone protein-HSC70

(heat shock cognate 71 kDa protein)-forming the HSC70-substrate complex, which binds lysosomal LAMP2A (lysosome-associated membrane protein type 2A) for subsequent lysosomal uptake and degradation (Qiao et al., 2021). Thus, autophagy, including mitophagy and CMA, is considered to be involved in the process of CBNPs-induced placental damage.

Furthermore, ferroptosis is confirmed to be involved in the progress of PM-induced damage. The findings showed that $PM_{2.5}$ induces ferroptosis in human endothelial cells (Wang and Tang, 2019), and lung epithelial cells (Guohua et al., 2021). Mitochondrial damage, mitophagy, and CMA are thought to be closely related to ferroptosis (Chen et al., 2021a; Yu et al., 2022). Ferroptosis is characterized by the small mitochondria with low condensed membrane densities, reduction or vanishing of crista, and outer membrane rupture for the mitochondria (Tang et al., 2021). So far, few reports about mitophagy and CMA in the process of particulate matter-induced injury have been reported. And few reports are related to the placenta. Thus, we wonder if mitophagy or CMA-related ferroptosis is involved in the CBNPs-induced placenta injury.

Above all, regarding of placental trafficking of carbon nanoparticles from the maternal side to the fetus and inducting placental toxicity, the study traced the CBNPs' targeting of red blood cells and mice's placenta. The study explored the placental toxicity caused by CBNPs *in vivo* and *in vitro*, respectively. The findings are expected to add some insight into understanding the risk aspect of CBNPs or toxicity of airborne PMs in the placenta regarding the further impaction on the fetus.

2. Methods

2.1. Characterization of CBNPs

To determine the nano-sized carbon black-induced placental toxicity, both 30 nm and 120 nm CBNPs were used in this study. 30 nm and 120 nm carbon black nanoparticles were obtained from Orion, Germany. Dynamic light scattering size and zeta potential of CBNPs were tested with Zetasizer Nano ZS90 (Malvern, Britain). Ultraviolet–visible spectroscopy (UV–Vis) absorption and fluorescence intensity (FL intensity) were determined by a microplate reader (Tecan Infinite E Plex, Switzerland) with reference to a previous study (Wu et al., 2022). BET area was provided by the manufacturer. The distribution of particle size was determined by Nano Measurer 1.2. CBNPs were ultrasonicated for >10 min before experiments to reduce agglomeration.

2.2. Animals and dose selection of CBNPs

All C57BL/6 mice (9–10 weeks old) were experimented with following the guidelines of the Xiamen University Institutional Committee for the Care and Use of Laboratory Animals (XMULAC20200188). Healthy C57BL/6 mice (15 female mice and 6 male mice) were purchased from the SLAC Laboratory Animal Center (Shanghai, China) and housed under specific pathogen-free conditions at Xiamen University Laboratory Animal Center (Xiamen, China). Mice had *ad libitum* access to food and water. After one week of acclimation, females and males spend the night in one cage for mating. The following morning, the

female with a vaginal plug or sperm observed on the vaginal smear was considered as gestational day 0.5 (GD0.5). The exposure pattern is consistent with that described in our previous study (Zhang et al., 2021). After anesthesia with isoflurane inhalation, the head and neck were backward exposed to the airway, and CBNPs suspension (5 mg/mL) 40 μL was slowly infused into the trachea of the pregnant mice. Saline, 30 nm CBNPs or 120 nm CBNPs were instilled on GD3.5, GD6.5, GD9.5, GD12.5, and GD15.5 (n = 5/group). All pregnant mice were sacrificed on GD18.5.

The dose used (200 µg/animal) in this study was chosen for the following reasons. First, the dose was based on the Chinese occupational exposure limit according to a previous study. The dose was further calculated as 1/2 of the maximum dose (He et al., 2020). Second, CBNPs were used to study as a core of PM2.5 (black carbon), the maximum of black carbon was $3 \mu g/m^3$ in the air (Chen et al., 2023; Liu et al., 2023b). Healthy adults inhale and exhale approximately 10 L of air every minute, and the total volume of air inhaled by the adult was about 14.4 m³/ day (10 L/min \times 60 min/h \times 24 h). Since approximately 90 % of the volume of air was exhaled during normal breathing, the adult inhaled about 4.32 μ g CBNPs/day (3 μ g/m³× 14.4 m³/day×10 %). The uncertainty factor was set at 100, with interspecies variation (10) and intraspecies variation (10) taken into account (He et al., 2020). Therefore, we calculated the doses $4.32 \,\mu\text{g}/\text{day} \times 3 \,\text{days} \times 100 = 1296 \,\mu\text{g}$. The dose was further calculated at about 1/6 of the maximum dose. Third, the exposure interval and dose referred to a previous study, which was used to demonstrate how CBNPs present in the lungs of heavy smokers and a highly ubiquitous pollutant generated from the combustion of organic matter promote lung cancer (Chang et al., 2022).

2.3. Cell culture and treatment

Human placental trophoblast cell line HTR-8/SVneo was established by introducing into first-trimester human trophoblasts the gene encoding simian virus 40 large T antigen and proved to be an important tool for the study of placental function (Graham et al., 1993). Human placental trophoblast cell line HTR-8/SVneo (MeisenCTCC, China) was cultured in RPMI 1640 Medium (Gibco, USA) supplemented with 10 % fetal bovine serum (Excell Bio, China) and 1 % Penicillin-Streptomycin (VivaCell, China). When cells reached 80 % confluence, cells were treated with 30 nm or 120 nm CBNPs for 24 h. To effectively inhibit ferroptosis, cells were pretreated with 30 µM ferrostatin-1 (MedChemExpress, China) for 2 h and then treated with 30 nm CBNPs at $100 \mu g/mL$ for 24 h. To demonstrate autophagy flux, 50 nM Bafilomycin A1 (an autophagy inhibitor, MedChemExpress) or 20 nm Rapamycin (an autophagy activator, MedChemExpress) was cotreated with 30 nm CBNPs at $100 \mu g/mL$ for 24 h.

2.4. RNA extraction and quantitative real-time polymerase chain reaction

Total RNA was extracted by using a TRIzol reagent (Sangon Biotech, China). All total RNA was of high purity with OD260/280 in the range of 1.8–2.0. The integrity of RNA was determined by agarose gel electrophoresis. RNA extracts were quantified using a multi-mode plate reader (Gene5, Biotek). 1000 ng RNA was reverse transcribed into mRNA by using PrimeScriptTM RT Master Mix (TaKaRa, #RR036A, Japan). The qRT-PCR was performed on a fluorescence quantitative PCR instrument real-time PCR system (Q towere3G, Germany) with the SYBR® Green Realtime PCR Master Mix (TOYOBO, #QPK-201) for 40 cycles. *GAPDH* or *Actb* was used as an internal control for mRNA. Primers are shown in Table S1.

2.5. Western blot

Tissues or cells were lysed with RIPA (Solarbio, China) supplemented with a 1 % Protease Inhibitor Cocktail, 1 % Phosphatase Inhibitor Cocktail I, and 1 % Phosphatase Inhibitor Cocktail II (MedChemExpress,

China). Supernatants were collected after a $12,000 \times \text{rpm}$ centrifuge for 10-20 min. Protein quantified by BCA kit (Beyotime, China) was denatured with 5 × SDS-PAGE loading buffer (with DTT) (Solarbio, China). 20-30 µg protein was separated with 8 %-12 % sodium dodecyl sulfate-polyacrylamide gel electrophoresis gels and transferred into a polyvinylidene fluoride membrane (PALL, USA). The bands were blocked with 5 % skimmed milk for 1 h at room temperature and incubated overnight at 4 °C with primary antibodies against GAPDH (Proteintech, 10494-1-AP, 1:10,000), DRP1 (Abclonal, A17069, 1:1000), Phospho-DRP1 (Ser637) (Beyotime, AF5791, 1:1000), SQSTM1/p62 (CST, #39749, 1:1000), LC3B (CST, #3868, 1:1000), PARKIN (Proteintech, 66674-1-Ig, 1:1000), GPX4 (Santa, sc-166570, 1:500) and MFN1 (Abclonal, A15474, 1:1000), MFN2 (Abclonal, A19678, 1:1000), OPA1 (Abclonal, A9833, 1:1000), FIS1 (Beyotime, AF8268, 1:1000), HSC70 (Beyotime, AF1132, 1:1000), LAMP1 (Beyotime, AF7353,1:1000), and LAMP2A (Beyotime, AF1036,1:1000). The bands were incubated with secondary antibodies (Thermofisher, 1:4000-1:10,000) for 1-1.5 h at room temperature. The bands were visualized using an ECL chemiluminescence detection system (Tanon 4600, China) and the intensity of the bands was quantified by Image J software (National Institutes of Health, USA).

2.6. Cell viability assay

The method was described in the previous study (Li et al., 2021). Cells were seeded in 96-well plates and incubated with 10 % CCK-8 solution (Biosharp, China) after exposure to 0, 10, 50, 100, 200, and 400 μ g/mL of CBNPs for 24 h. Optical density was determined by a microplate reader at 450 nm (Varioskan Flash, Thermo Fisher Scientific) after incubating with CCK-8 solution for 30 min.

2.7. Oxidative stress and lipid peroxidation detection

Cells were seeded in the 10-cm dish, and collected with 0.25 % trypsin (VivaCell, China) after exposure. The method was used in a previous study (Wei et al., 2020a). The level of glutathione, oxidized glutathione (GSSG), and malondialdehyde (MDA) in the lysates were measured with GSH and GSSG Assay Kit (Beyotime, China), and Lipid Peroxidation Malondialdehyde (MDA) Assay Kit (Beyotime, China) according to the manufacturer's instructions. The optical density was detected by a microplate (Varioskan Flash, Thermo Fisher Scientific).

2.8. mtDNA copy number detection

Cells were seeded in a 6-well plate, and collected with 0.25 % trypsin after exposure. DNA was extracted using TaKaRa MiniBEST Universal Genomic DNA Extraction Kit Ver 5.0 (TaKaRa, #9765, Japan). mtDNA copy numbers were determined by the Human Mitochondrial DNA Monitoring Primer Set (TaKaRa, #7246). All total DNA was of high purity with OD260/280 in the range of 1.80–1.90. The integrity of DNA was determined by agarose gel electrophoresis. The quantitative real-time polymerase chain reaction was performed on a fluorescence quantitative PCR instrument real-time PCR system (ABI7500, Applied Biosystems, USA) with the TB Green Premix Ex Taq II (Tli RNaseH Plus) (Takara, Japan) for 40 cycles. 50 ng genomic DNA was used per reaction.

2.9. Reactive oxygen species (ROS) detection

Cells were seeded in 96-well black-walled plates and treated with 10, 25, 50, and 100 μ g/mL CBNPs. Cells were incubated with 10 μ M DCFHDA (Sigma, USA) for 30 min after CBNPs exposure. The fluorescence was detected using a microplate reader (Varioskan Flash, Thermo Fisher Scientific, USA) at ex488/em525.

2.10. Mitochondrial membrane potential (MMP) detection

Cells were seeded in confocal dishes. MMP was detected with a mitochondrial membrane potential assay kit with JC-1 (Beyotime, China). Cells were stained with JC-1 staining solution for 20 min at 37 $^{\circ}$ C, washed with PBS, and observed with Laser confocal microscopy (Nikon A1R, Japan) at ex488/em525 and ex561/em590.

2.11. Transmission electron microscope (TEM)

For CBNPs, 0.1 mg/mL CBNPs were dropped into copper grids and allowed to adsorb for 10 min. The excess sample solution was removed, and the copper mesh was stained with 1 % uranyl acetate for 15 s. The sample was allowed to air-dry at room temperature for 3 h and then observed using a transmission electron microscope. For cells, red blood cells, or tissues, the method was consistent with the previous study (Wei et al., 2020a). Here, we made some minor modifications. Cells were seeded in 6-cm dishes, collected with 0.25 % trypsin, and fixed in 2.5 % glutaraldehyde. For red blood cells, blood was collected and centrifuged at 3000 ×g for 15 min. The bottom layer is red blood cells. Red blood cells were cut into small pieces and fixed in 2.5 % glutaraldehyde. Tissues were cut into small pieces and fixed in 2.5 % glutaraldehyde. Cells or tissues were washed with 1 × PB, fixed with 1 % OsO₄, and dehydrated with graded alcohol. Acetone replacement was performed at room temperature and tissues or cells were embedded in resin, and cut using an ultramicrotome (Leica, German). The sections were mounted on copper grids, stained with uranyl acetate and lead citrate, and then observed with a transmission electron microscope (HT-7800, Hitachi, Japan, or G2 Spirit Biotwin, Tecnai Spirit, Netherlands).

2.12. Plasmid transfection

Cells were seeded on confocal dishes overnight. 1.5 μ g pCMV-GFP-LC3B or pCMV-mCherry-GFP-LC3B (Beyotime, China) was transfected with HighGene transfection reagent (Abclonal, China) before treatment with CBNPs.

2.13. Mitochondria and lysosome labeling

The method referred to a previous study (Chen et al., 2021b). Cells were seeded into confocal dishes and exposed to CBNPs. Cells were incubated in 200 nM Mitotracker (ThermoFisher) and 200 nM Lyso-Tracker (ThermoFisher) for 30 min at 37 $^{\circ}$ C after exposure. The fluorescence was located with confocal microscopy (Zeiss LSM 880, German) at ex488/em525 and ex561/em590. When mitochondria are wrapped by lysosomes, red light and green light overlap to form yellow light.

2.14. Calcein-AM and PI staining

Cells were seeded into confocal dishes and exposed to CBNPs. Cells were incubated in 2 μ M Calcein-AM (Yeasen, China) and 4.5 μ M PI (Yeasen, China) for 15 min at 37 °C after exposure. The fluorescence was located with confocal microscopy (Zeiss LSM 880, German).

2.15. Immunochemistry

Placenta slices were dewaxed and placed in a 1 \times Tris-EDTA (0.1 mM EDTA, pH 6.0) and boiled for 15 min for antigen repair. Then, the slices were blocked with 5 % bovine serum albumin at 37 °C for 1 h and incubated with primary antibody (Ki67, 1:100, Servicebio, GB111141) overnight at 4 °C. On the second day, after rewarming for 50 min, the slides were washed three times with PBS and reacted with a secondary antibody for 50 min, added DAB, and stained with hematoxylin for 2 min.

2.16. Dark-field hyperspectral imaging (HSI)

Dark-field hyperspectral imaging was a novel strategy for visualizing and tracing nanoparticles. The method used in this study referred to previous studies (Wang et al., 2023; Cary et al., 2023). Placentas were separated from pregnant mice and immersed in fixed liquid (Servicebio, China). The fresh tissue was fixed over 24 h, dehydrated with gradient alcohol and xylene, embedded with wax, and cut into 5 µm sections. Sections were dewaxed and sealed with resin. HSI was performed with a CytoViva darkfield microscope equipped with a pixelFly CCD camera. ENVI 4.8 software was used to capture and process the images and to acquire spectra. The dark-field images were captured and then scanned for HSI. We shot with 15× eyepieces and $60\times$ objectives. CBNPs alone were used to acquire the spectral library of CBNPs with a region of interest function of ENVI 4.8. The placenta is divided into the decidua, junctional layer, and labyrinth layer. Three areas were taken pictures separately. Spectral libraries obtained from CBNPs were filtered with 12 control pictures (3 pictures/area, n = 4). The remaining spectral libraries were used for spectral angle mappers.

2.17. Statistical analysis

Most data were presented as the mean \pm SD where possible. Comparisons between the two groups were performed using one-way ANOVA followed by the LSD test. CCK-8 assay and ROS assay were tested with two-way ANOVA. Statistical analysis was performed using SPSS 19.0. The data were considered significant when a value of P < 0.05 or P < 0.01.

3. Results

3.1. Characterization of CBNPs

TEM images of CBNPs were shown in Fig. 1A and C. A total of 50 particles were measured. Fig. 1A and B showed that the average size of CBNPs was approximately 30 nm. Fig. 1C and D showed that the average size of CBNPs was approximately 120 nm. And BET area for 30 nm CBNPs was $103 \text{ m}^2/\text{g}$, and for 120 nm CBNPs was $20 \text{ m}^2/\text{g}$ (Fig. 1E). The average dynamic light scattering size of 30 nm CBNPs and 120 nm CBNPs in different dispersed solutions was shown in Fig. 1F, and G. Both 30 nm and 120 nm CBNPs in normal saline and PBS formed larger sizes, indicating CBNPs easily got agglomerated in normal saline and PBS. The zeta potential of 30 nm and 120 nm CBNPs in four solvents was all negative. The average zeta potential of 30 nm CBNPs was -56.3 mV in water. The average zeta potential of 120 nm CBNPs was -28.0 mV in water (Fig. 1H, I). For UV-Vis absorption, a peak of 30 nm and 120 nm CBNPs was found at 560 nm in the medium. (Fig. 1J, K). When assessing their photoluminescence, a fluorescence intensity peak was found in RPMI 1640 medium solvents (The emission wavelength of 30 nm carbon black in the medium was 440 nm) (Fig. 1L, M).

3.2. CBNPs entered the mice's placenta and caused fetal growth restriction

A schematic of animal experimental design was shown in Fig. 2A. To determine whether maternal exposure to CBNPs during gestation resulted in adverse outcomes in placentas and fetuses, mice were sacrificed after CBNPs exposure on GD18.5. As shown in Fig. 2B–D, maternal weight decreased after 120 nm CBNPs exposure. Though the number of fetuses did not manifest a significant change, the fetal body length and body weight decreased upon both 30 nm and 120 nm CBNPs exposure (Fig. 2C–E). Of note, both 30 nm and 120 nm CBNPs were deposited in the maternal lungs upon exposure, and lung weight remained unchanged (Fig. S1). They could also be found in red blood cells detected by TEM (Fig. 2F) and placenta detected by HSI (Fig. 2G, H). The placenta was an important organ for the exchange of nutrients

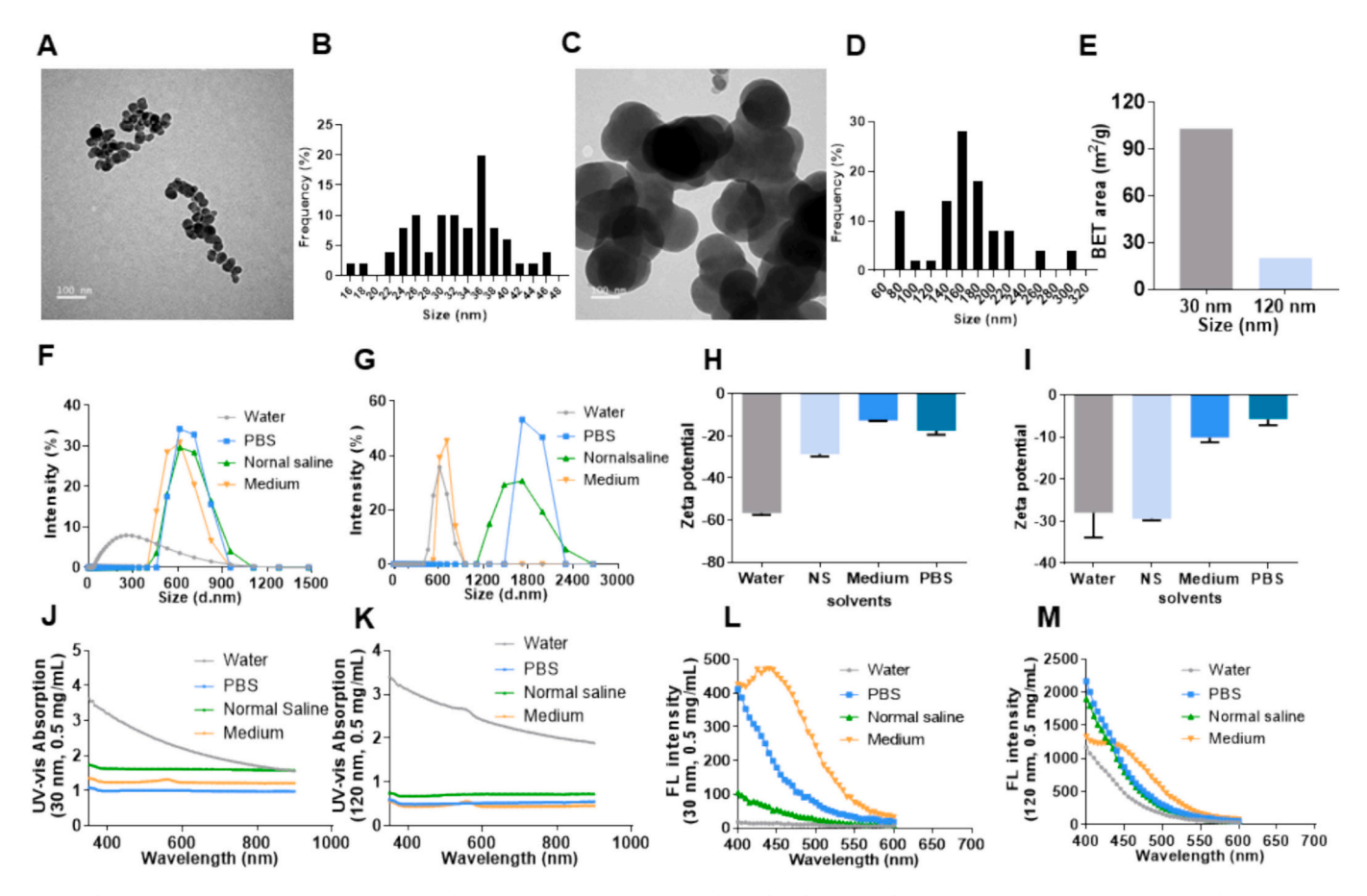


Fig. 1. Characterization of CBNPs. (A) TEM image of 30 nm CBNPs. (B) Histogram of size-distribution analysis of 30 nm CBNPs. (C) TEM image of 120 nm CBNPs. (D) Histogram of size-distribution analysis of 120 nm CBNPs. (E) BET area of CBNPs. (F) Distribution of 30 nm CBNPs DLS size in different solvents. (G) Distribution of 120 nm CBNPs DLS size in different solutions. (H) Zeta potential of 30 nm CBNPs in different solvents (n = 3). (I) Zeta potential of 120 nm CBNPs in different solvents (n = 3). (I) UV-vis absorption of 30 nm CBNPs in different solutions. (L) Fluorescence of 30 nm CBNPs in different solutions (excitation wavelength = 350 nm). (M) Fluorescence of 120 nm CBNPs in different solutions. (excitation wavelength = 350 nm).

and wastes. Interestingly, 30 nm CBNPs could be found in the both junctional zone and labyrinth zone, and 120 nm CBNPs could only be discovered in the labyrinth zone. The results proved that CBNPs could flow into the placenta by blood circulation, which was demonstrated in Fig. 2I. The results indicated that CBNPs, which were instilled through the trachea, entered the bloodstream through the lungs and then entered the placenta. Taken together, we found that CBNPs could enter the mice's placenta and further lead to fetal growth restriction.

3.3. CBNPs exposure during gestation caused mitochondrial injury, disabled autophagy, and ferroptosis in mice's placenta

To investigate the potential mechanism of placental injury after CBNPs exposure, the ultrastructure of the placenta was observed by TEM. The images manifested that the morphology of mitochondria was observably altered due to the CBNPs exposure. There are a lot of damaged mitochondria in the placenta upon CBNPs exposure, reflected by the diminishment of the mitochondrial matrix and mitochondrial cristae (Fig. 3A). The balance of mitochondrial fission and fusion is of importance to mitochondrial quality. So, we examined the mitochondrial fission protein (FIS1, DRP1, and pDRP1(Ser637)) and mitochondrial fusion protein (MFN1, MFN2, and OPA1) in mice's placenta after CBNPs exposure. Mitochondrial fission protein FIS1 increased and pDRP1(Ser637) decreased upon both 30 nm and 120 nm CBNPs exposure (Fig. 3B, C). The results demonstrated that CBNPs exposure devastated placental mitochondria via enhancing mitochondrial fission mice's placenta, which was mainly through the DRP1

dephosphorylation at the site of Ser637 and the increase of FIS1.

Mitophagy is a pathway to eliminate damaged mitochondria. CMA is a pathway to selectively degrade protein in lysosomes to maintain cell homeostasis. Mitophagy-related protein (PARKIN) decreased upon 30 nm and 120 nm CBNPs exposure. CMA-related protein (LC3BII, P62, and LAMP2A) elevated after 30 nm and 120 nm CBNPs exposure, while HSC70 decreased upon 120 nm CBNPs exposure (Fig. 3D, E). Due to mitochondrial damage and autophagy were both found to result in ferroptosis, we examined ferroptosis-related indexes. GPX4 protein was only found to descend upon 120 nm CBNPs (Fig. 3F). *Gpx4* and *Scl7a11* mRNA decreased in both 30 nm and 120 nm CBNPs (Fig. 3G, H). Ki67 staining showed that cell proliferation declined upon 30 nm and 120 nm CBNPs exposure in mice's placentas (Fig. 3I). The results suggested that the unbalanced mitochondrial homeostasis and disrupted autophagy could result in ferroptosis upon CBNPs exposure in mice's placenta.

3.4. CBNPs exposure caused mitochondrial dysfunction in human placental trophoblast cells

To investigate the potential mechanism of the toxicity of 30 nm and 120 nm CBNPs in the placenta, we used human placental trophoblast cells to explore potential mechanisms *in vitro*. HTR-8/SVneo cells exposed to 30 nm and 120 nm CBNPs caused a significant decrease in cell viability *in vitro* (Fig. 4A). Next, we explored the ROS and mitochondrial membrane potential. The results manifested that both 30 nm and 120 nm CBNPs caused an increase in ROS level and a decrease in MMP reflected by the decreased red fluorescence and the increased

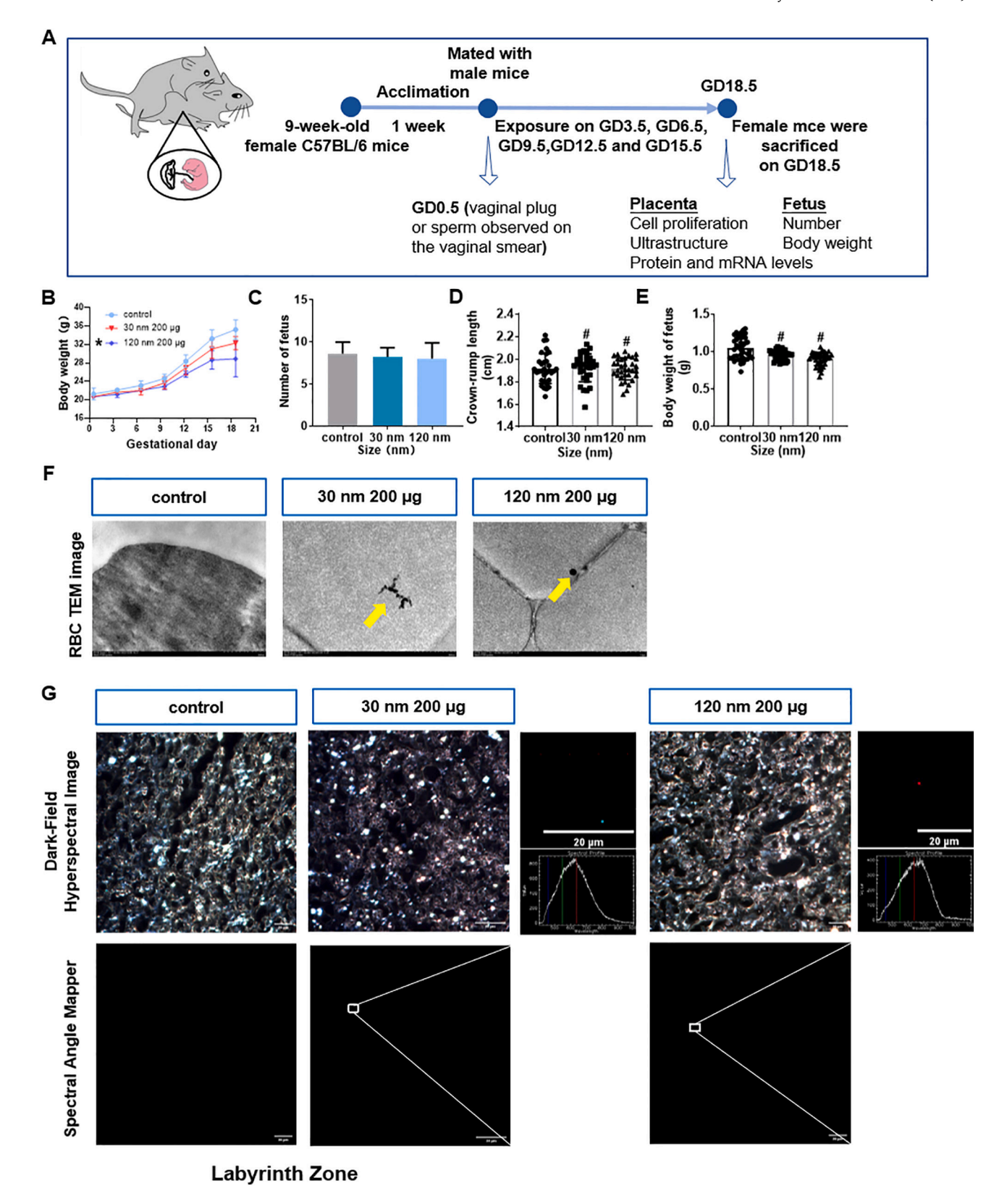


Fig. 2. CBNPs entered the mice's placenta and caused fetal growth restriction. (A) Schematic of animal experimental design. (B) Maternal body weight decreased upon 120 nm CBNP exposure. (n = 3–4) (C) The number of fetus remained unchanged. (D) CBNPs exposure during gestation caused fetal crown-rump length decline. (n = 4) (E) CBNPs exposure during gestation caused fetal body weight decline. (n=4) (F) TEM images of red blood cells. (G, H) Dark-field hyperspectral mages of mice's placenta. (I) Structure of placenta and mouse labyrinth zone. Scale bar = 20 μ m. Data were presented as the mean \pm SD. *: P < 0.05, #: P < 0.01 vs. corresponding control.

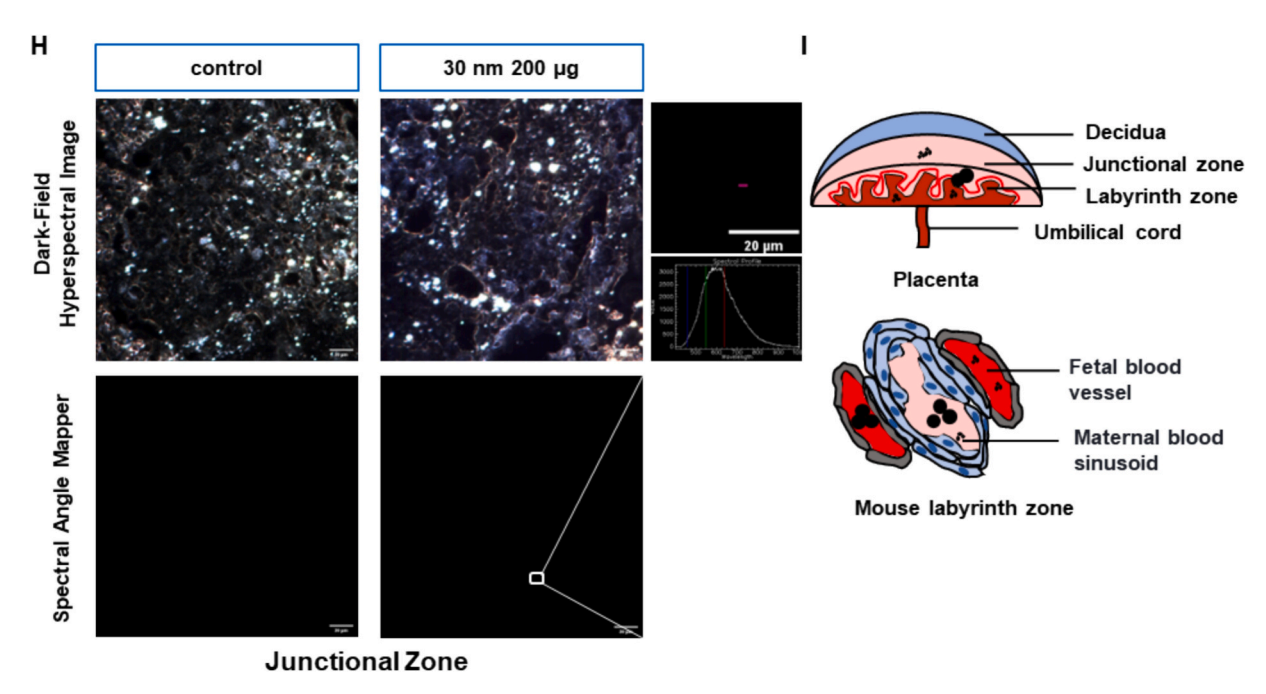


Fig. 2. (continued).

green fluorescence (Fig. 4B, C). Subsequently, mitochondrial fission and fusion protein were also tested *in vitro*. As shown in Fig. 4D, E, pDRP1 (Ser637) reduced in the 30 nm CBNPs group. And mitochondrial fusion protein remained unchanged. Besides, 30 nm CBNPs caused a significant decrease in mtDNA copy number (Fig. 4F). Furthermore, the cellular ultrastructure of HTR8-Svneo cells was observed (Fig. 4G). TEM images showed the disappearance of mitochondrial crista and matrix upon CBNPs exposure. The images manifested that CBNPs exposure caused mitochondrial damage. In addition, CBNPs could be seen in the lysosomes, which demonstrated that CBNPs could be swallowed by the lysosome, and may affect the function of lysosome. The results indicated that CBNPs exposure could cause mitochondrial fission and mitochondrial dysfunction *in vitro*.

3.5. CBNPs exposure caused inactivated autophagy in human placental trophoblast cells

Based on the results above, the mitophagy and CMA-related proteins were also determined after CBNPs exposure in vitro. We found LC3BII, P62, and LAMP2A increased both in the 30 nm and 120 nm. PARKIN decreased after 30 nm exposure, and HSC70 decreased after 30 nm and 120 nm CBNPs exposure (Fig. 5A, B). Furthermore, the fluorescence of GFP-LC3B (green dots) was heightened obviously in the CBNPs-treated groups (Fig. 5C). In addition, mCherry-GFP-LC3B fluorescence was one way to reflect the autophagy flux. After the formation of autophagolysosome, GFP fluorescence (green) was quenched in an acidic environment, but mCherry fluorescence (red) was not affected. Our results showed that CBNPs exposure did not eliminate green fluorescence and yellow dots (GFP and mCherry colocalization) increased, indicating that autophagy was blocked in the process of formation of autolysosomes by both 30 nm and 120 nm CBNPs (Fig. 5D). The mitochondria and lysosomes labeling suggested the increased lysosomes upon 30 nm and 120 nm CBNPs exposure. Besides, no obvious colocalization was found between mitochondria and lysosomes (Fig. 5E). The result suggested that autophagy was inactivated by CBNPs exposure.

3.6. CBNPs exposure caused ferroptosis in human placental trophoblast cells

Mitochondrial damage and disabled autophagy were related to

ferroptosis. To investigate the ferroptosis caused by 30 nm and 120 nm CBNPs in vitro, cells were treated with 30 nm and 120 nm CBNPs treatment at 100 μg/mL, respectively. GPX4 protein and ferroptosis-related mRNA (*GPX4* and *SLC7A11*) decreased upon 30 nm CBNPs exposure (Fig. 6A–C). The changes in ROS, lipid peroxidation, and GSH level are hallmarks of ferroptosis. GSH: GSSG declined upon 30 nm CBNPs exposure (Fig. 6D). MDA as a parameter of lipid peroxidation increased upon 30 nm CBNPs exposure (Fig. 6E). Propidium iodide (PI) is a red-fluorescent cell viability dye that is excluded from live cells as it is impermeable to the cell membrane. Calcein-AM is a cell-staining reagent that can fluorescently label living cells. Calcein-AM/PI staining indicated cell death/cell damage was caused by both 30 nm and 120 nm CBNPs (Fig. 6F). These results showed that CBNPs could cause ferroptosis in human placental trophoblast cells.

Based on the above results, ferrostatin-1, as a specific inhibitor for ferroptosis was used to ameliorate the ferroptosis caused by 30 nm CBNPs. These results indicated that CBNPs-induced ferroptosis could be reversed by ferrostatin-1, reflected by the increased cell viability, GSH: GSSG level, GPX4 protein, *GPX4* and *SCL7A11* mRNA, and the decreased ROS and MDA content (Fig. 6G–M). The results further confirmed that ferroptosis could be triggered by CBNPs in human placental trophoblasts.

3.7. Rapamycin promoted autophagy and inhibited ferroptosis in CBNPstreated human placental trophoblast cells

Our results demonstrated that CBNPs exposure caused notable autophagy suppression and ferroptosis in mice's placentas and human trophoblast cells. To investigate whether autophagy and ferroptosis influenced cell homeostasis, an activator of autophagy, rapamycin was used to promote autophagy and inhibit ferroptosis. 30 nm CBNPs were cotreated with rapamycin to verify the mechanism as an *in vitro* model. Notably, rapamycin cotreatment enhanced autophagy and inhibited ferroptosis upon 30 nm CBNPs exposure (Fig. 7A–D). The results manifested that cell death, cell viability, and ROS could be recovered by rapamycin (Fig. 7E–G). Bafilomycin cotreatment inhibited autophagy and promoted ferroptosis upon 30 nm CBNPs exposure (Fig. S2). These results illustrated that ferroptosis could be relieved by rapamycin in human placental trophoblast cells upon 30 nm CBNPs exposure. The results further confirmed autophagy suppression was the main cause of

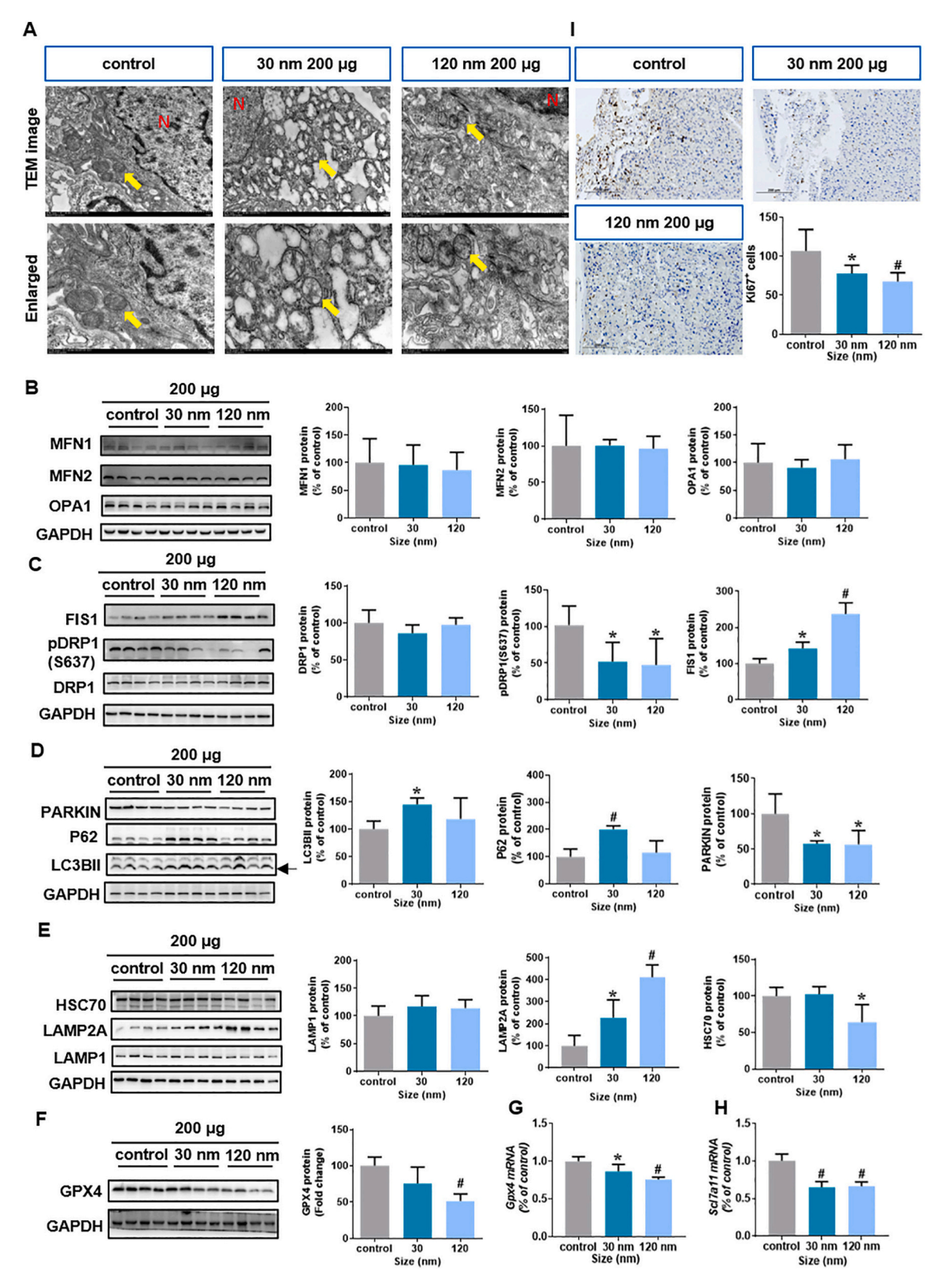


Fig. 3. CBNPs exposure during gestation caused mitochondrial injury, disabled autophagy, and ferroptosis in mice's placenta. (A) TEM images of mice's placentas. Yellow arrow: mitochondria, N (red): cell nucleus. (B) Mitochondrial fusion protein remained unchanged upon CBNPs exposure (n = 4). (C) Mitochondrial fission protein increased upon CBNPs exposure (n = 4). (D, E) CBNPs caused disrupted autophagy in mice's placenta. (F–H) GPX4 protein decreased upon CBNPs exposure (n = 4). Ferroptosis-related mRNA (*Gpx4* and *Slc7a11* mRNA) decreased upon CBNPs exposure (n = 4). (I) Cell proliferation decreased upon CBNPs exposure reflected by a decrease of Ki67⁺ cells in mice's placenta (n = 4). scale bar = 100 μm. All data were presented as the mean \pm SD. *: P < 0.05, #: P < 0.01 vs. corresponding control.

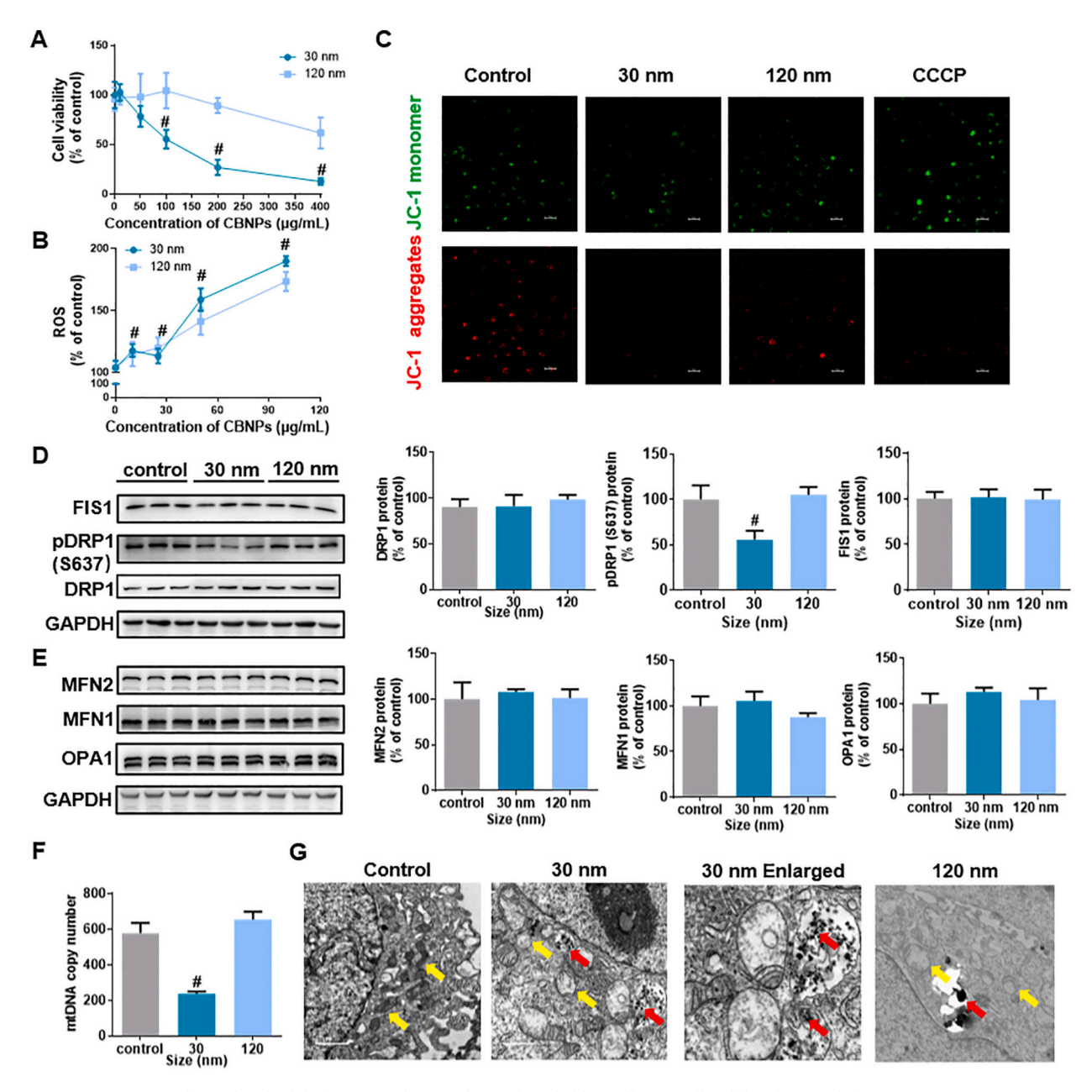


Fig. 4. CBNPs exposure caused mitochondrial dysfunction in human placental trophoblast cells. (A) Cell viability decreased after exposure to CBNPs (n = 4). (B) ROS level increased after exposure to CBNPs detected by a microplate reader (n = 4). (C) Mitochondrial membrane potential decreased after exposure to CBNPs. Scale bar = 50 μ m. (D) Mitochondrial fission protein (pDRP1 (S637)) declined upon 30 nm CBNPs exposure (n = 3). (E) Mitochondrial fusion protein (OPA1, MFN1, MFN2) remained unchanged upon CBNPs exposure (n = 3). (F) Mitochondrial DNA copy number decreased after exposure to 30 nm CBNPs (n = 3). (G) TEM image of HTR-8/SVneo cells indicated mitochondrial damage upon CBNPs exposure. Red arrow: CBNPs. Yellow arrow: mitochondria. Scale bar = 1 μ m. All data were presented as the mean \pm SD. #: P < 0.01 vs. corresponding control as indicated.

ferroptosis after CBNPs exposure in human placental trophoblast cells.

4. Discussion

Due to its small size, nanomaterial can play different physiological effects when compared with bulky material. The smaller size of $PM_{0.1}$ can generate greater threats to public health due to the greater surface area and reactivity compared with the fine particles ($PM_{2.5}$) (Mukherjee and Agrawal, 2018; Terzano et al., 2010). Furthermore, as the core of the airborne particulate matters, carbon-related particles were found in cord blood, confirming the ability of these particles to cross the placenta and enter the fetal circulation system (Bongaerts et al., 2022). Maternal inhalation of carbon black nanoparticles could induce

neurodevelopmental changes in mouse offspring (Umezawa et al., 2018), increase preterm birth (Fang et al., 2022), and induce liver DNA damage in the mothers and the *in-utero* exposed offspring (Jackson et al., 2012). Besides, few studies have focused on the core of $PM_{2.5}$ or CBNPs induced toxicity in the placenta. Hence, we traced the CBNPs and investigated the nano-sized carbon black particles-induced toxicity in the placenta, which could improve our understanding of the CBNPs toxicity in the placenta and even fetal growth restriction.

In this study, preliminary experiments have showed that $50 \mu g/mice$ CBNPs significantly influenced placental mitochondria, however, no significant change for fetal body weight and GPX4 protein expression has been observed (Fig. S3). To trace the mitochondrial effect related potential fetal outcome, pregnant mice were exposed to an increased

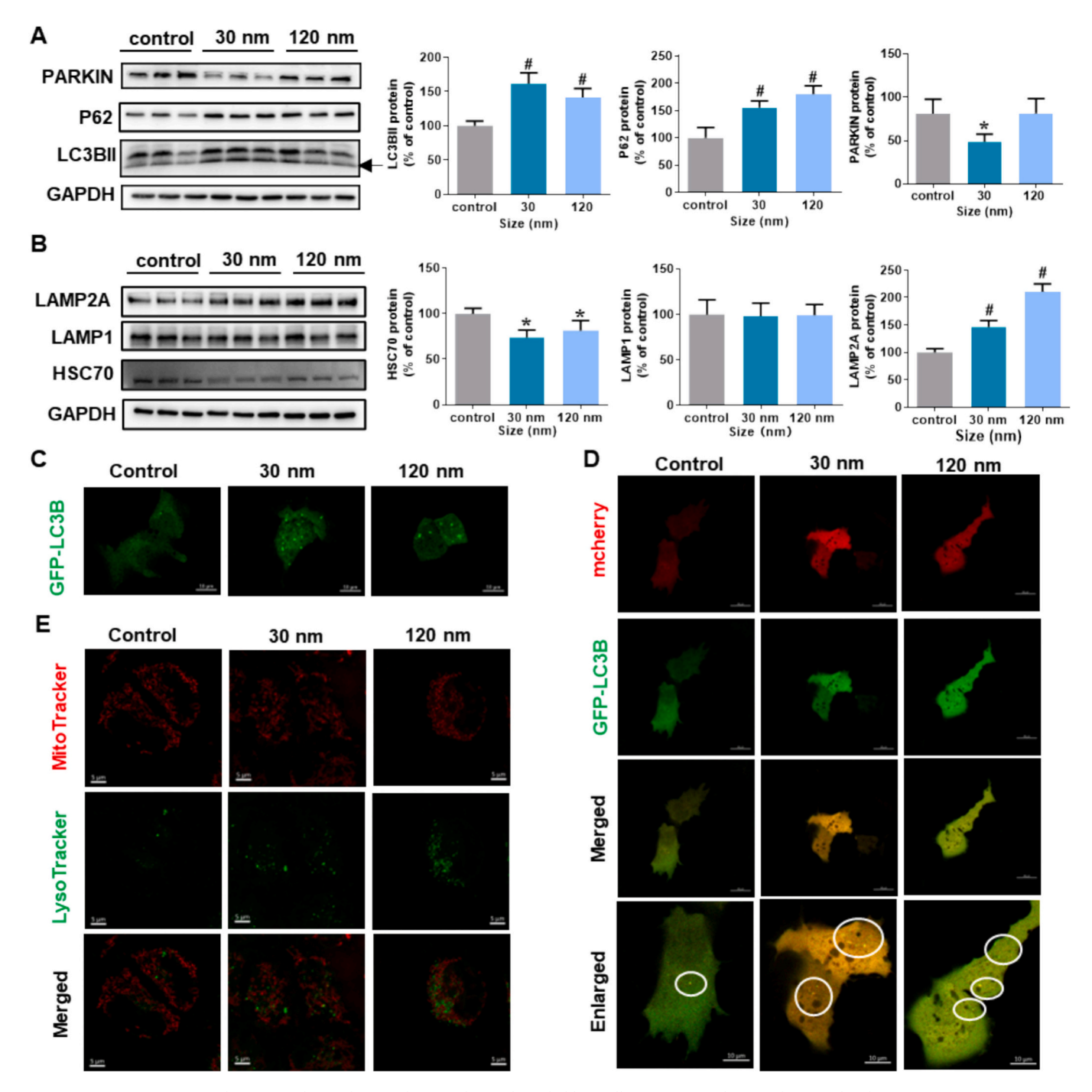


Fig. 5. CBNPs exposure caused inactivated autophagy in human placental trophoblast cells. (A, B) Mitophagy and CMA-related protein (LC3BII, P62, PARKIN, LAMP2A, and HSC70) changed in human placental trophoblast cells after exposure to CBNPs (n = 3). (C) GFP-LC3B fluorescence (green dots) increased upon CBNPs exposure. Scale bar = 20 μ m. (D) mCherry-GFP-LC3B fluorescence (yellow dots: red dots and green dots colocalization) increased upon CBNPs exposure. (E) Mitochondrial and lysosomal markers did not show significant fusion upon CBNPs exposure. Scale bar = 5 μ m. All data were presented as the mean \pm SD. *: P < 0.05, #: P < 0.01 vs. corresponding control as indicated.

200 µg CBNPs of 30 nm and 120 nm. The high doses have showed us a comprehensive profile of toxic characterization of CBNPs from maternal exposure to fetal adverse outcome during pregnancy, which may be the mechanism supporting for the epidemiological observations (Lakshmanan et al., 2015; van Rossem et al., 2015).

After exposure, both 30 nm and 120 nm CBNPs were deposited in the maternal lungs and first found in red blood cells traced by TEM and mice's placenta traced by HSI. We have reasoned that CBNPs can enter the blood vessels from the lungs and circulate to the placenta. Red blood cells may be the transport carriers of CBNPs into other organs. Red blood

cells were reported to inspire strategies for nanomedicine (Zhang et al., 2022). Here, we found red blood cells could also load CBNPs into other organs. Furthermore, CBNPs exposure caused the reduction of placental cell proliferation, and fetal growth restriction, suggesting that placental and fetal health were dramatically interfered with CBNPs.

We put forward that the two-hit hypothesis may play a vital importance in the placenta upon CBNPs exposure. The first hit to the placenta is mitochondria upon CBNPs exposure. Mitochondrial damage is thought to be one of the main causes of placental dysfunction (Deyssenroth et al., 2021; Brunst et al., 2022). To explore the potential

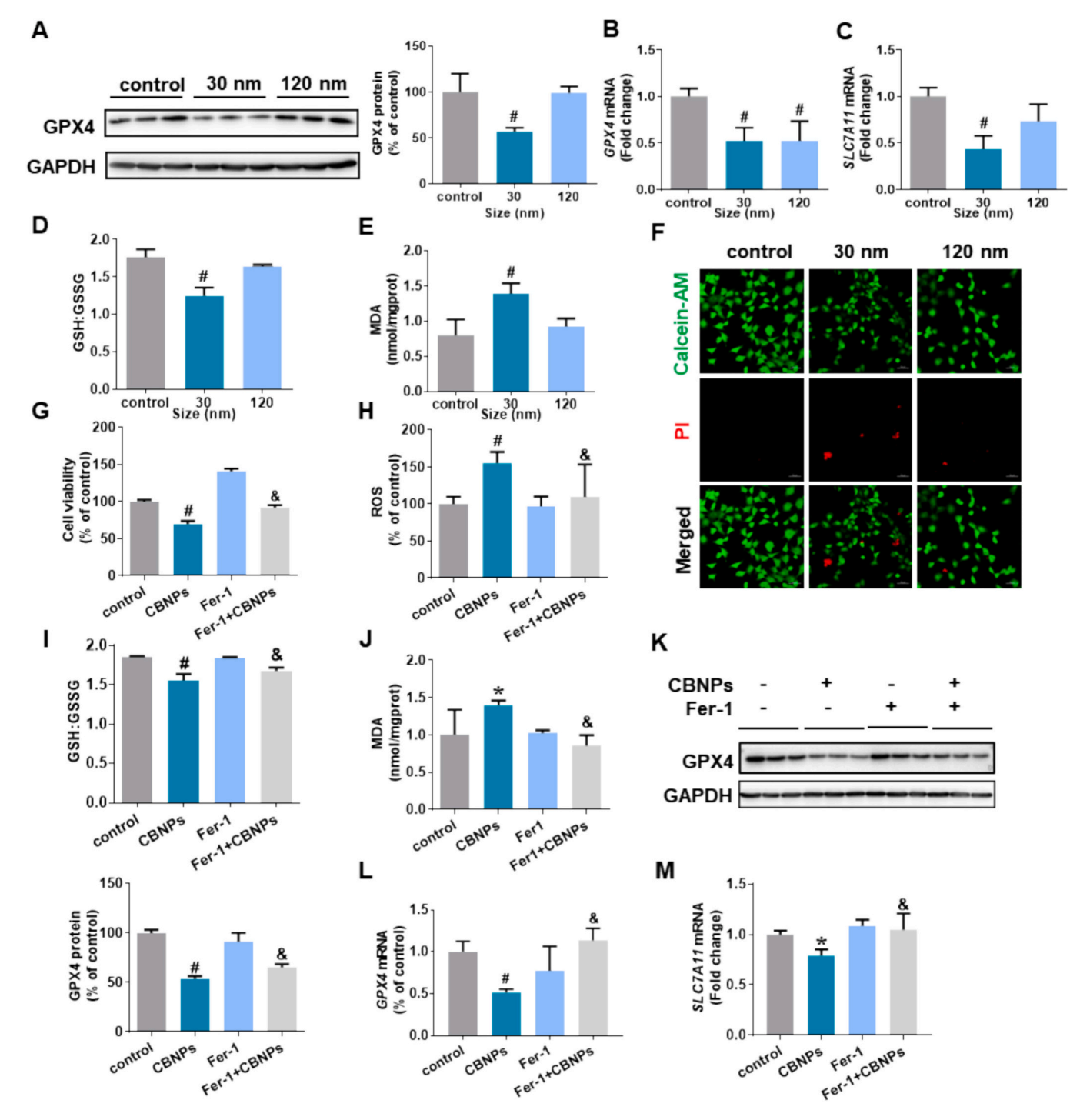


Fig. 6. CBNPs exposure caused ferroptosis in human placental trophoblast cells. (A) GPX4 protein went down after exposure to 30 nm CBNPs (n = 3). (B, C) Ferroptosis-related mRNA (GPX4 and SLC7A11 mRNA) changed after exposure to CBNPs (n = 3). (D) GSH:GSSG level declined after exposure to 30 nm CBNPs (n = 3). (E) MDA content increased after exposure to 30 nm CBNPs (n = 3). (F) Calcein-AM/PI staining indicated CBNPs caused cell death of human placental trophoblast cells. (G) Ferrostatin-1 promoted cell viability upon CBNPs exposure (n = 4). (H) ROS level went down by ferrostatin-1 detected by a microplate reader (n = 4). (I) GSH:GSSG level, (J) MDA content, (K) GPX4 protein, and (L, M) ferroptosis-related mRNA (GPX4 and SLC7A11 mRNA) were reversed by ferrostatin-1 (n = 3). All data were presented as the mean \pm SD. *: P < 0.05, #: P < 0.01 vs. corresponding control. &: P < 0.05 vs. 30 nm CBNPs group.

mechanism of CBNPs-induced placental damage, the ultrastructure of the placental cells upon CBNPs exposure was observed *in vivo* and *in vitro*. The morphology of mitochondria has changed dramatically *in vivo* and *in vitro*. The decrease in mitochondrial membrane potential and mtDNA damage were the manifestations of mitochondrial dysfunction (Li et al., 2019; Zou et al., 2021). We found that mitochondrial membrane potential decreased after 30 nm and 120 nm CBNPs exposure.

mtDNA copy number decreased after exposure to 30 nm CBNPs in human placental trophoblast cells. In addition, phosphorylation of DRP1 at the 637 site reduced after CBNPs exposure, which indicated CBNPs caused excessive mitochondrial fission/fragmentation (Yang et al., 2020). Mitochondrial fragmentation would lead to oxidative phosphorylation imbalance and even cell death (Sprenger and Langer, 2019). Abnormal phosphorylation of Drp1 promotes excessive mitochondrial

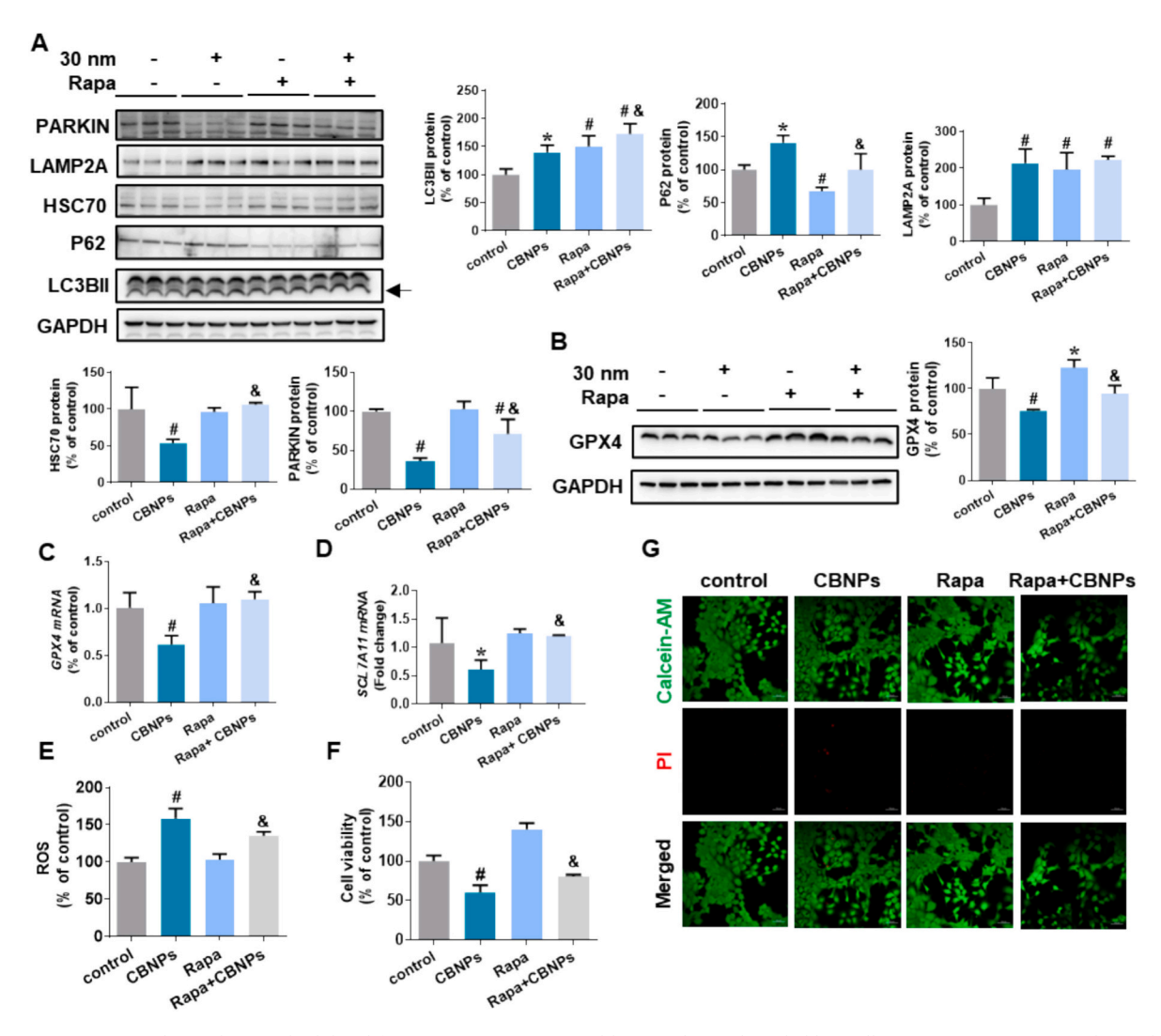


Fig. 7. Rapamycin promoted autophagy and inhibited ferroptosis in CBNPs-treated human placental trophoblast cells. (A) Rapamycin promoted autophagy upon CBNPs exposure. (B–D) Rapamycin increased GPX4 protein and ferroptosis-related mRNA expression upon CBNPs exposure. (E) Rapamycin reduced ROS production upon CBNPs exposure. (F) Rapamycin increased cell viability upon CBNPs exposure. (G) Rapamycin mitigated cell death (red) caused by CBNPs. All data were presented as the mean \pm SD. *: P < 0.05, #: P < 0.01 vs. corresponding control as indicated. &: P < 0.05 vs. 30 nm CBNPs group.

fragmentation, which is also associated with placental dysfunction (Ausman et al., 2018). Our results demonstrated that CBNPs caused placental mitochondrial dysfunction.

The second hit to the placenta is inactivated autophagy upon CBNPs exposure. Mitophagy is a selective autophagic process that degrades non-functional mitochondrial fragments produced by fission (Kurihara et al., 2012). Clearance of damaged mitochondria via mitophagy is significant in preventing cells from oxidative imbalance (Livingston et al., 2019). Here, the decline of PARKIN upon CBNPs exposure manifested the suppression of mitophagy (Ashrafi and Schwarz, 2013). CMA regulates intracellular homeostasis by degrading damaged or harmful proteins. CMA-related protein, HSC70 went down, indicating CAM was also suppressed by CBNPs. Meanwhile, the autophagy flux indicator, mCherry-GFP-LC3B, and mitochondria-lysosome labeling, together with the results of rapamycin or bafilomycin A1 cotreatment with CBNPs demonstrated that CBNPs could inhibit the formation of autolysosomes and inhibit the clearance of damaged mitochondria and damaged protein. The results hinted that CBNPs inhibited autophagy, which resulted in obstacles in the elimination of damaged mitochondria and damaged proteins, and finally caused an imbalance in cell homeostasis.

Ferroptosis was also distinguished upon CBNPs exposure as the result of two-hit of CBNPs in the placenta. Ferroptosis is considered a type of

mitochondria-related or autophagy-related cell death (Yu et al., 2022; Zhou et al., 2020). Ferroptosis is a recently observed way of regulating cell death, and it has been proved that mitochondrial dysfunction could lead to ferroptosis in arsenic-induced pancreatic injuries and graphene quantum dots-induced neurotoxicity (Wei et al., 2020b; Wu et al., 2020). Currently, GPX4, lipid peroxidation, and ROS are biomarkers to identify ferroptosis (Wei et al., 2020b), which may be coupled with the changes of Slc7a1l, Acls4, or other genes (Guohua et al., 2021; Zhou et al., 2020). Cystine transporter SLC7A11 could give rise to cystine uptake, which subsequently promotes both GPX4 protein synthesis and GSH synthesis (Dodson et al., 2019). Our data revealed that cell viability decreased after 30 nm CBNPs exposure at 100 µg/mL or higher concentrations. ROS level, MDA content increased, and GSH/GSSG ratio decreased after exposure to 30 nm CBNPs in human placental trophoblast cells. GPX4 protein and ferroptosis-related genes changed after CBNPs exposure in vivo and in vitro. Moreover, ferroptosis is characterized morphologically by the small mitochondria with condensed mitochondrial membrane densities, reduction or vanishing of mitochondria crista, and outer mitochondrial membrane rupture (Xie et al., 2016). In this study, the mitochondrial morphology in TEM images showed similar changes in vivo and in vitro. Ferrostatin-1, the specific inhibitor of ferroptosis, alleviated environmental chemicals-induced ferroptosis (Wei et al., 2020b; Zeng et al., 2021), involving nanoparticles (Qin et al., 2021). Ferrostatin-1 was found to lighten the ferroptosis induced by 30 nm CBNPs in HTR-8/SVneo cells. Rapamycin could enhance autophagy and inhibit ferroptosis. Hence, our findings suggested that CBNPs exposure could lead to ferroptosis and eventually cause fetal growth restriction. The results may result from two-hit of CBNPs, mitochondrial dysfunction, and the depression of autophagy in the placenta, respectively.

Previous studies have shown that PM caused oxidative stress or inflammation on pregnant mice or placental cells. Few studies focused on the adverse outcomes or the mechanism of placental injury caused by PM (Table S2). Compared with the previous research, as a core of PM simulant or tobacco combustion or industrial product, CBNPs were confirmed to cause fetal growth restriction. We put forward the "two-hit" hypothesis of placental injury caused by CBNPs. The study provides an in-depth look at the potential developmental toxicity of CBNPs exposure during pregnancy and provides a key empirical basis for this area. These findings cannot be ignored for the formulation of a safe exposure dose threshold and risk assessment of pregnant women.

The limitation of the study includes some potential toxicities that are ambiguous when illustrating the tests *in vitro* and *in vivo*, respectively. For example, even though 30 nm CBNPs induced more severe injuries *in vitro*, the damages seemed to be more apparent *in vivo*. However, placental cell proliferation *in vivo* and fetal body weight had no significant difference between the 30 nm and 120 nm CBNPs groups. Therefore, some additional information needs to be further addressed regarding the CBNPs' morphology and toxicology, especially their size-dependent bio-molecular modification (*i.e.*, protein corona), interaction (cell surface receptor clustering) and their toxicokinetics (*i.e.*, cellular uptake and internalization) *in vivo* and *in vitro*.

Taken together, this study identified that CBNPs caused placental injury *via* two-hit of CBNPs, including mitochondrial damage and inactivated autophagy-derived ferroptosis, thereby causing fetal growth restriction.

CRediT authorship contribution statement

Jing Li: Writing – original draft, Visualization, Validation, Software, Methodology, Investigation, Formal analysis, Data curation, Conceptualization. Hongying Gao: Writing – review & editing, Validation, Methodology, Investigation, Formal analysis. Zehua Xu: Visualization, Validation, Software, Methodology, Investigation, Data curation. Biling Gao: Visualization, Validation, Software, Methodology. Liang Zhang: Validation, Software, Methodology. Bowen Su: Methodology, Investigation. Shijing Yang: Methodology. Jiangling Liu: Methodology. Ya Liu: Methodology. Xiuxiu Wang: Methodology. Heng Wang: Resources. Yi Lin: Writing – review & editing, Supervision, Project administration, Funding acquisition, Conceptualization. Heqing Shen: Writing – review & editing, Supervision, Project administration, Funding acquisition, Conceptualization.

Funding

This work was supported by the National Natural Science Foundation of China (Nos. 22076158, 21177123, 91543113, 21777157, and 82073505) and the Natural Science Foundation of Fujian Province (No. 2023J02004).

Declaration of competing interest

The authors declare that they have no known competing financial interests or personal relationships that could have appeared to influence the work reported in this paper.

Acknowledgments

The authors appreciate the technical assistance of Yao Luming, Wu Caiming, Liu Qingfeng, You Xiang, and Huang Jingru from the Core Facility of Biomedical Sciences, Xiamen University (Xiamen, China).

Appendix A. Supplementary data

Supplementary data to this article can be found online at https://doi.org/10.1016/j.scitotenv.2024.178167.

Data availability

Data will be made available on request.

References

- Andrade-Guel, M., Reyes-Rodríguez, P.Y., Cabello-Alvarado, C.J., Cadenas-Pliego, G., Ávila-Orta, C.A., 2022. Influence of modified carbon black on nylon 6 nonwoven fabric and performance as adsorbent material. Nanomaterials 12, 23. https://doi. org/10.3390/nano12234247.
- Ashrafi, G., Schwarz, T.L., 2013. The pathways of mitophagy for quality control and clearance of mitochondria. Cell Death Differ. 20 (1), 31–42. https://doi.org/
- Ausman, J., Abbade, J., Ermini, L., Farrell, A., Tagliaferro, A., Post, M., et al., 2018. Ceramide-induced BOK promotes mitochondrial fission in preeclampsia. Cell Death Dis. 9 (3), 298. https://doi.org/10.1038/s41419-018-0360-0.
- Bacakova, L., Pajorova, J., Tomkova, M., Matejka, R., Broz, A., Stepanovska, J., et al., 2020. Applications of nanocellulose/nanocarbon composites: focus on biotechnology and medicine. Nanomaterials 10, 2. https://doi.org/10.3390/nano10020196.
- Bongaerts, E., Lecante, L.L., Bové, H., Roeffaers, M.B.J., Ameloot, M., Fowler, P.A., et al., 2022. Maternal exposure to ambient black carbon particles and their presence in maternal and fetal circulation and organs: an analysis of two independent population-based observational studies. Lancet Planet. Health 6 (10), e804–e811. https://doi.org/10.1016/s2542-5196(22)00200-5.
- Bové, H., Bongaerts, E., Slenders, E., Bijnens, E.M., Saenen, N.D., Gyselaers, W., et al., 2019. Ambient black carbon particles reach the fetal side of human placenta. Nat. Commun. 10 (1), 3866. https://doi.org/10.1038/s41467-019-11654-3.
- Brunella, V., Rossatto, B.G., Scarano, D., Česano, F., 2021. Thermal, morphological, electrical properties and touch-sensor application of conductive carbon black-filled polyamide composites. Nanomaterials 11, 11. https://doi.org/10.3390/nano11113103.
- Brunst, K.J., Hsu, H.L., Zhang, L., Zhang, X., Carroll, K.N., Just, A., et al., 2022. Prenatal particulate matter exposure and mitochondrial mutational load at the maternal-fetal interface: effect modification by genetic ancestry. Mitochondrion 62, 102–110. https://doi.org/10.1016/j.mito.2021.11.003.
- Cary, C.M., DeLoid, G.M., Yang, Z.N., Bitounis, D., Polunas, M., Goedken, M.J., et al., 2023. Ingested polystyrene nanospheres translocate to placenta and fetal tissues in pregnant rats: potential health implications. Nanomaterials 13, 4. https://doi.org/ 10.3390/nano13040720.
- Chang, C.Y., You, R., Armstrong, D., Bandi, A., Cheng, Y.T., Burkhardt, P.M., et al., 2022. Chronic exposure to carbon black ultrafine particles reprograms macrophage metabolism and accelerates lung cancer. Sci. Adv. 8 (46), eabq0615. https://doi.org/ 10.1126/sciadv.abq0615.
- Chen, C., Wang, D., Yu, Y., Zhao, T., Min, N., Wu, Y., et al., 2021a. Legumain promotes tubular ferroptosis by facilitating chaperone-mediated autophagy of GPX4 in AKI. Cell Death Dis. 12 (1), 65. https://doi.org/10.1038/s41419-020-03362-4.
- Chen, N., Guo, Z., Luo, Z., Zheng, F., Shao, W., Yu, G., et al., 2021b. Drp1-mediated mitochondrial fission contributes to mitophagy in paraquat-induced neuronal cell damage. Environ. Pollut. 272, 116413. https://doi.org/10.1016/j. envpol.2020.116413.
- Chen, Y.W., Cheng, Y.H., Hsu, C.Y., 2023. Characterization of the sources and health risks of polycyclic aromatic hydrocarbons in PM_{2.5} and their relationship with black carbon: a case study in northern Taiwan. Environ. Pollut. 336, 122427. https://doi. org/10.1016/j.envpol.2023.122427.
- Chen, Z.H., Wu, Y.F., Wang, P.L., Wu, Y.P., Li, Z.Y., Zhao, Y., et al., 2016. Autophagy is essential for ultrafine particle-induced inflammation and mucus hyperproduction in airway epithelium. Autophagy 12 (2), 297–311. https://doi.org/10.1080/15548627.2015.1124224.
- Deng, X., Zhang, F., Rui, W., Long, F., Wang, L., Feng, Z., et al., 2013. PM_{2.5}-induced oxidative stress triggers autophagy in human lung epithelial A549 cells. Toxicol. In Vitro 27 (6), 1762–1770. https://doi.org/10.1016/j.tiv.2013.05.004.
- Deyssenroth, M.A., Rosa, M.J., Eliot, M.N., Kelsey, K.T., Kloog, I., Schwartz, J.D., et al., 2021. Placental gene networks at the interface between maternal PM_{2.5} exposure early in gestation and reduced infant birthweight. Environ. Res. 199, 111342. https://doi.org/10.1016/j.envres.2021.111342.
- Dodson, M., Castro-Portuguez, R., Zhang, D.D., 2019. NRF2 plays a critical role in mitigating lipid peroxidation and ferroptosis. Redox Biol. 23, 101107. https://doi. org/10.1016/j.redox.2019.101107.
- Fang, J., Yang, Y., Zou, X., Xu, H., Wang, S., Wu, R., et al., 2022. Maternal exposures to fine and ultrafine particles and the risk of preterm birth from a retrospective study in

- Beijing, China. Sci. Total Environ. 812, 151488. https://doi.org/10.1016/j.ccitateavy 2021 151488
- Gillmore, T., Farrell, A., Alahari, S., Sallais, J., Kurt, M., Park, C., et al., 2022. Dichotomy in hypoxia-induced mitochondrial fission in placental mesenchymal cells during development and preeclampsia: consequences for trophoblast mitochondrial homeostasis. Cell Death Dis. 13 (2), 191. https://doi.org/10.1038/s41419-022-04641-y
- Graham, C.H., Hawley, T.S., Hawley, R.G., MacDougall, J.R., Kerbel, R.S., Khoo, N., et al., 1993. Establishment and characterization of first trimester human trophoblast cells with extended lifespan. Exp. Cell Res. 206 (2), 204–211. https://doi.org/10.1006/excr.1993.1139.
- Guohua, F., Tieyuan, Z., Xinping, M., Juan, X., 2021. Melatonin protects against PM_{2.5}-induced lung injury by inhibiting ferroptosis of lung epithelial cells in a Nrf2-dependent manner. Ecotoxicol. Environ. Saf. 223, 112588. https://doi.org/10.1016/i.ecoepy.2021.112588.
- He, M., Jiang, X., Zou, Z., Qin, X., Zhang, S., Guo, Y., et al., 2020. Exposure to carbon black nanoparticles increases seizure susceptibility in male mice. Nanotoxicology 14 (5), 595–611. https://doi.org/10.1080/17435390.2020.1728412.
- Hou, L., Guan, S., Jin, Y., Sun, W., Wang, Q., Du, Y., et al., 2020. Cell metabolomics to study the cytotoxicity of carbon black nanoparticles on A549 cells using UHPLC-Q/ TOF-MS and multivariate data analysis. Sci. Total Environ. 698, 134122. https://doi. org/10.1016/j.scitotenv.2019.134122.
- Jackson, P., Hougaard, K.S., Boisen, A.M., Jacobsen, N.R., Jensen, K.A., Møller, P., et al., 2012. Pulmonary exposure to carbon black by inhalation or instillation in pregnant mice: effects on liver DNA strand breaks in dams and offspring. Nanotoxicology 6 (5), 486–500. https://doi.org/10.3109/17435390.2011.587902.
- Kaushik, S., Cuervo, A.M., 2018. The coming of age of chaperone-mediated autophagy. Nat. Rev. Mol. Cell Biol. 19 (6), 365–381. https://doi.org/10.1038/s41580-018-0001-6
- Kurihara, Y., Kanki, T., Aoki, Y., Hirota, Y., Saigusa, T., Uchiumi, T., et al., 2012. Mitophagy plays an essential role in reducing mitochondrial production of reactive oxygen species and mutation of mitochondrial DNA by maintaining mitochondrial quantity and quality in yeast. J. Biol. Chem. 287 (5), 3265–3272. https://doi.org/ 10.1074/jbc.M111.280156.
- Lakshmanan, A., Chiu, Y.H., Coull, B.A., Just, A.C., Maxwell, S.L., Schwartz, J., et al., 2015. Associations between prenatal traffic-related air pollution exposure and birth weight: modification by sex and maternal pre-pregnancy body mass index. Environ. Res. 137, 268–277. https://doi.org/10.1016/j.envres.2014.10.035.
- Li, J., Wang, J., Wang, Y.L., Luo, Z., Zheng, C., Yu, G., et al., 2021. NOX2 activation contributes to cobalt nanoparticles-induced inflammatory responses and Tau phosphorylation in mice and microglia. Ecotoxicol. Environ. Saf. 225, 112725. https://doi.org/10.1016/j.ecoenv.2021.112725.
- Li, Z., Fu, J., Li, Z., Tang, Y., Hua, Q., Liu, L., et al., 2019. Air pollution and placental mitochondrial DNA copy number: mechanistic insights and epidemiological challenges. Environ. Pollut. 255 (Pt 2), 113266. https://doi.org/10.1016/j. envpol.2019.113266.
- Liu, H., Lai, W., Nie, H., Shi, Y., Zhu, L., Yang, L., et al., 2023a. PM_{2.5} triggers autophagic degradation of Caveolin-1 via endoplasmic reticulum stress (ERS) to enhance the TGF-β1/Smad3 axis promoting pulmonary fibrosis. Environ. Int. 181, 108290. https://doi.org/10.1016/j.envint.2023.108290.
- Liu, J., Li, S., Fei, X., Nan, X., Shen, Y., Xiu, H., et al., 2022. Increased alveolar epithelial TRAF6 via autophagy-dependent TRIM37 degradation mediates particulate matterinduced lung metastasis. Autophagy 18 (5), 971–989. https://doi.org/10.1080/ 15548627.2021.1965421.
- Liu, J., Liu, R., Zhang, Y., Lao, X., Mandeville, K.L., Ma, X., et al., 2023b. Leisure-time physical activity mitigated the cognitive effect of PM_{2.5} and PM_{2.5} components exposure: evidence from a nationwide longitudinal study. Environ. Int. 179, 108143. https://doi.org/10.1016/j.envint.2023.108143.
- Livingston, M.J., Wang, J., Zhou, J., Wu, G., Ganley, I.G., Hill, J.A., et al., 2019. Clearance of damaged mitochondria via mitophagy is important to the protective effect of ischemic preconditioning in kidneys. Autophagy 15 (12), 2142–2162. https://doi.org/10.1080/15548627.2019.1615822.
- Maltepe, E., Fisher, S.J., 2015. Placenta: the forgotten organ. Annu. Rev. Cell Dev. Biol. 31, 523–552. https://doi.org/10.1146/annurev-cellbio-100814-125620.
- Manojlović-Stojanoski, M., Borković-Mitić, S., Nestorović, N., Ristić, N., Trifunović, S., Stevanović, M., et al., 2022. The effects of BSA-stabilized selenium nanoparticles and sodium selenite supplementation on the structure, oxidative stress parameters and selenium redox biology in rat placenta. Int. J. Mol. Sci. 23, 21. https://doi.org/10.3390/ijms232113068.
- Mukherjee, A., Agrawal, M., 2018. A global perspective of fine particulate matter pollution and its health effects. Rev. Environ. Contam. Toxicol. 244, 5–51. https://doi.org/10.1007/398_2017_3.
- Qiao, L., Ma, J., Zhang, Z., Sui, W., Zhai, C., Xu, D., et al., 2021. Deficient chaperone-mediated autophagy promotes inflammation and atherosclerosis. Circ. Res. 129 (12), 1141–1157. https://doi.org/10.1161/circresaha.121.318908.
- Qin, X., Zhang, J., Wang, B., Xu, G., Yang, X., Zou, Z., et al., 2021. Ferritinophagy is involved in the zinc oxide nanoparticles-induced ferroptosis of vascular endothelial cells. Autophagy 17 (12), 4266–4285. https://doi.org/10.1080/ 15548627.2021.1911016.
- van Rossem, L., Rifas-Shiman, S.L., Melly, S.J., Kloog, I., Luttmann-Gibson, H., Zanobetti, A., et al., 2015. Prenatal air pollution exposure and newborn blood pressure. Environ. Health Perspect. 123 (4), 353–359. https://doi.org/10.1289/ abs.1307419.
- Sferruzzi-Perri, A.N., Higgins, J.S., Vaughan, O.R., Murray, A.J., Fowden, A.L., 2019. Placental mitochondria adapt developmentally and in response to hypoxia to support

- fetal growth. Proc. Natl. Acad. Sci. USA 116 (5), 1621–1626. https://doi.org/10.1073/pnas.1816056116.
- Sprenger, H.G., Langer, T., 2019. The good and the bad of mitochondrial breakups. Trends Cell Biol. 29 (11), 888–900. https://doi.org/10.1016/j.tcb.2019.08.003.
- Tang, D., Chen, X., Kang, R., Kroemer, G., 2021. Ferroptosis: molecular mechanisms and health implications. Cell Res. 31 (2), 107–125. https://doi.org/10.1038/s41422-020-00441-1.
- Terzano, C., Di Stefano, F., Conti, V., Graziani, E., Petroianni, A., 2010. Air pollution ultrafine particles: toxicity beyond the lung. Eur. Rev. Med. Pharmacol. Sci. 14 (10), 809–821.
- Torrinha, Á., Oliveira, T., Ribeiro, F.W.P., Correia, A.N., Lima-Neto, P., Morais, S., 2020. Application of nanostructured carbon-based electrochemical (bio)sensors for screening of emerging pharmaceutical pollutants in waters and aquatic species: a review. Nanomaterials 10, 7. https://doi.org/10.3390/nano10071268.
- Umezawa, M., Onoda, A., Korshunova, I., Jensen, A., Koponen, I.K., Jensen, K.A., et al., 2018. Maternal inhalation of carbon black nanoparticles induces neurodevelopmental changes in mouse offspring. Part. Fibre Toxicol. 15 (1), 36. https://doi.org/10.1186/s12989-018-0272-2.
- Van Pee, T., Hogervorst, J., Dockx, Y., Witters, K., Thijs, S., Wang, C., et al., 2023. Accumulation of black carbon particles in placenta, cord blood, and childhood urine in association with the intestinal microbiome diversity and composition in four- to six-year-old children in the ENVIRONAGE birth cohort. Environ. Health Perspect. 131 (1), 17010. https://doi.org/10.1289/ehp11257.
- Wang, X.D., Xu, L.N., Ma, M.H., Xu, M., Zhou, Q.F., Liu, S.J., et al., 2023. A novel strategy for visualizing, tracing, and measuring the gastrointestinal absorption of silver nanoparticles. Adv. Funct. Mater. https://doi.org/10.1002/adfm.202302366.
- Wang, Y., Tang, M., 2019. PM2.5 induces ferroptosis in human endothelial cells through iron overload and redox imbalance. Environ. Pollut. 254 (Pt A), 112937. https://doi. org/10.1016/j.envpol.2019.07.105.
- Wei, J., Hao, Q., Chen, C., Li, J., Han, X., Lei, Z., et al., 2020a. Epigenetic repression of miR-17 contributed to di(2-ethylhexyl) phthalate-triggered insulin resistance by targeting Keap1-Nrf2/miR-200a axis in skeletal muscle. Theranostics 10 (20), 9230–9248. https://doi.org/10.7150/thno.45253.
- Wei, S., Qiu, T., Yao, X., Wang, N., Jiang, L., Jia, X., et al., 2020b. Arsenic induces pancreatic dysfunction and ferroptosis via mitochondrial ROS-autophagy-lysosomal pathway. J. Hazard. Mater. 384, 121390. https://doi.org/10.1016/j. ihazmat.2019.121390.
- Wu, T., Liang, X., Liu, X., Li, Y., Wang, Y., Kong, L., et al., 2020. Induction of ferroptosis in response to graphene quantum dots through mitochondrial oxidative stress in microglia. Part. Fibre Toxicol. 17 (1), 30. https://doi.org/10.1186/s12989-020-00363-1.
- Wu, T., Wang, X., Cheng, J., Liang, X., Li, Y., Chen, M., et al., 2022. Nitrogen-doped graphene quantum dots induce ferroptosis through disrupting calcium homeostasis in microglia. Part. Fibre Toxicol. 19 (1), 22. https://doi.org/10.1186/s12989-022-00464-z
- Wu, X., Li, J., Wang, S., Jiang, L., Sun, X., Liu, X., et al., 2021. 2-Undecanone protects against fine particle-induced kidney inflammation via inducing mitophagy. J. Agric. Food Chem. 69 (17), 5206–5215. https://doi.org/10.1021/acs.jafc.1c01305.
- Xie, Y., Hou, W., Song, X., Yu, Y., Huang, J., Sun, X., et al., 2016. Ferroptosis: process and function. Cell Death Differ. 23 (3), 369–379. https://doi.org/10.1038/ cdd.2015.158.
- Xu, Y.Y., Liu, Y., Cui, L., Wu, W.B., Quinn, M.J., Menon, R., et al., 2021. Hypoxic effects on the mitochondrial content and functions of the placenta in fetal growth restriction. Placenta 114, 100–107. https://doi.org/10.1016/j. placenta.2021.09.003.
- Yang, D., Zhu, J., Zhou, X., Pan, D., Nan, S., Yin, R., et al., 2022. Polystyrene micro- and nano-particle coexposure injures fetal thalamus by inducing ROS-mediated cell apoptosis. Environ. Int. 166, 107362. https://doi.org/10.1016/j.envint.2022.107362.
- Yang, L., Li, X., Jiang, A., Li, X., Chang, W., Chen, J., et al., 2020. Metformin alleviates lead-induced mitochondrial fragmentation via AMPK/Nrf2 activation in SH-SY5Y cells. Redox Biol. 36, 101626. https://doi.org/10.1016/j.redox.2020.101626.
- Yu, F., Zhang, Q., Liu, H., Liu, J., Yang, S., Luo, X., et al., 2022. Dynamic O-GlcNAcylation coordinates ferritinophagy and mitophagy to activate ferroptosis. Cell Discov. 8 (1), 40. https://doi.org/10.1038/s41421-022-00390-6.
 Zeng, L., Zhou, J., Wang, X., Zhang, Y., Wang, M., Su, P., 2021. Cadmium attenuates
- Zeng, L., Zhou, J., Wang, X., Zhang, Y., Wang, M., Su, P., 2021. Cadmium attenuates testosterone synthesis by promoting ferroptosis and blocking autophagosomelysosome fusion. Free Radic. Biol. Med. 176, 176–188. https://doi.org/10.1016/j. freeradbiomed.2021.09.028.
- Zhang, E., Phan, P., Algarni, H.A., Zhao, Z., 2022. Red blood cell inspired strategies for drug delivery: emerging concepts and new advances. Pharm. Res. 39 (11), 2673–2698. https://doi.org/10.1007/s11095-022-03328-5.
- Zhang, Q., Zhang, C., Ge, J., Lv, M.W., Talukder, M., Guo, K., et al., 2020. Ameliorative effects of resveratrol against cadmium-induced nephrotoxicity via modulating nuclear xenobiotic receptor response and PINK1/Parkin-mediated mitophagy. Food Funct. J. 11 (2), 1856–1868. https://doi.org/10.1039/c9fo02287b.
- Zhang, X., Zhang, J., Wu, Y., Nan, B., Huang, Q., Du, X., et al., 2021. Dynamic recovery after acute single fine particulate matter exposure in male mice: effect on lipid deregulation and cardiovascular alterations. J. Hazard. Mater. 414, 125504. https:// doi.org/10.1016/j.jhazmat.2021.125504.
- Zhao, Y., Wang, P., Zhou, Y., Xia, B., Zhu, Q., Ge, W., et al., 2021. Prenatal fine particulate matter exposure, placental DNA methylation changes, and fetal growth. Environ. Int. 147, 106313. https://doi.org/10.1016/j.envint.2020.106313.
- Zhong, G., Wan, F., Wu, S., Jiang, X., Tang, Z., Zhang, X., et al., 2021. Arsenic or/and antimony induced mitophagy and apoptosis associated with metabolic abnormalities

and oxidative stress in the liver of mice. Sci. Total Environ. 777, 146082. https://doi. org/10.1016/j.scitotenv.2021.146082.

Zhou, B., Liu, J., Kang, R., Klionsky, D.J., Kroemer, G., Tang, D., 2020. Ferroptosis is a type of autophagy-dependent cell death. Semin. Cancer Biol. 66, 89–100. https://doi.org/10.1016/j.semcancer.2019.03.002.

Zou, R.A.-O., Tao, J., Qiu, J., Shi, W.A.-O., Zou, M.A.-O., Chen, W.A.-O., et al., 2021. Ndufs1 deficiency aggravates the mitochondrial membrane potential dysfunction in pressure overload-induced myocardial hypertrophy. Oxidative Med. Cell. Longev. 2021, 5545261. https://doi.org/10.1155/2021/5545261.